Efficiency Evaluation of Receiving Current Control Using Pulse Density Modulation for Dynamic Wireless Power Transfer

Sakahisa Nagai
Graduate School of Frontier Sciences
The University of Tokyo
Kashiwa, Japan
nagai-saka@edu.k.u-tokyo.ac.jp

Toshiyuki Fujita
Graduate School of Frontier Sciences
The University of Tokyo
Kashiwa, Japan
t-fujita@edu.k.u-tokyo.ac.jp

Hiroshi Fujimoto
Graduate School of Frontier Sciences
The University of Tokyo
Kashiwa, Japan
fujimoto@ k.u-tokyo.ac.jp

Shogo Tsuge
TOYOTA MOTOR CORPOLATION
Susono, Japan
shogo_tsuge@mail.toyota.co.jp

Toshiya Hashimoto
TOYOTA MOTOR CORPOLATION
Susono, Japan
toshiya_hashimoto@mail.toyota.co.jp

***Abstract*— Dynamic wireless power transfer (DWPT) for electric vehicles (EVs) is an innovative technique that enables the EVs to enhance the driving range and reduce the capacity of the battery. The receiving current control is important to prevent the battery from overcharging. In this paper, the receiving current control using an active rectifier is focused on. Pulse density modulation (PDM) is effective in terms of the switching loss in the rectifier compared with pulse width modulation. In the previous papers regarding to the PDM, the operation is evaluated in stationary WPT systems. In this paper, the transmission energy efficiency of the receiving current control with the PDM is evaluated using a high-speed rotational testbench for the DWPT. In addition, centralized PDM (CPDM) and distributed PDM (DPDM) are experimentally compared. As a result, it was confirmed that the current control performances using the CPDM and DPDM are the same in spite of the mutual inductance dynamic change at 40 km/h. The energy efficiency of the DPDM was 3.3–7.9% higher compared with one of the CPDM because it can reduce the filter current and loss in the filter inductance. Therefore, the DPDM is effective for the receiving current control of the DWPT system.**

Keywords*— dynamic wireless power transfer, pulse density modulation, current control, energy efficiency

I. INTRODUCTION

Penetration ratio of electric vehicles (EVs) are increasing all over the world because they do not emit carbon dioxide while driving [1]. However, they still have some problems such as a short driving range, long battery charging time, and expensiveness. One of the solutions is a dynamic wireless power transfer (DWPT) technique [2]. The energy consumption while driving is wirelessly charged; therefore, the driving range can be massively enhanced. In addition, the battery capacity can be reduced. Hence the vehicle weight, cost, and charging time can be reduced [3].

The power control of the WPT system is studied for the purposes of achieving high-efficient power transmission and protecting the battery from overcharging. It is well-known that the WPT efficiency depends on the voltage and current of the transmitter and receiver coils. By controlling them, the high-efficient WPT can be achieved [4], [5]. In [4] and [5], the receiving power is controlled with high efficiency by controlling a DC-DC converter on the transmitter side or receiver side. In [6], the receiver side is controlled as a constant power load by using an active rectifier. In [7], three phase inverter for three phase WPT system is controlled to maximize the efficiency.

For the second purpose, the receiver power is reduced for the battery protection. The static WPT system is classified by Society of Automotive Engineers International in J2954 [8]. The WPT system is divided into three power classes: WPT-1 for 3.6 kW, WPT-2 for 7.7 kW, and WPT-3 for 11 kW. The received power should be controlled by the size of the car and the state of charge of the battery to prevent the battery from overcharging. Especially, the quick receiving current control is needed for the WPT to hybrid EVs because the battery capacity is small.

This paper focuses on the receiving current control in terms of the second point. For the vehicle application, the receiver side equipment should be simple and lightweight; therefore, an active rectifier is used in the control. In addition, pulse density modulation (PDM) is considered in the switching of the rectifier since the switching loss can be zero [9]. The previous papers regarding to the PDM discussed the performance in stationary WPT systems. In this paper, the PDM is experimentally evaluated using a high-speed rotational DWPT testbench. In addition, two types of the PDM are compared from the viewpoint of the transmission energy efficiency.

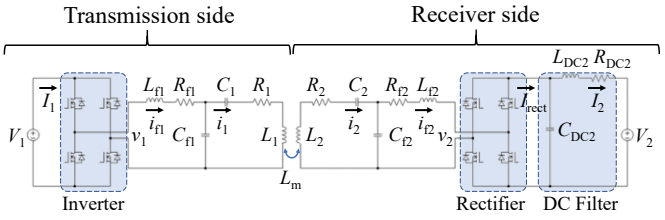

Fig. 1. Circuit diagram of magnetic resonant WPT using double-sided LCC.

This paper is organized as follows: Section II explains the double-sided LCC WPT circuit [10], [11] used in the experiments. Section III explains the two types of the PDM. Section IV describes the receiving current controller. Section V shows the experimental results of the current control using the high-speed rotational DWPT testbench. Finally, Section VI concludes this paper.

II. Wireless Power Transfer Circuit

This section describes the magnetic resonant WPT circuit used in this paper. Fig. 1 shows the circuit diagram which consists of a DC voltage source, full bridge inverter, double-sided LCC WPT part [10], [11], active rectifier, and DC filter. V, v, I, i, R, L, and C denote DC voltage, high-frequency voltage, DC current, high-frequency current, internal resistance, inductance, and capacitance, respectively. The subscripts '1', '2', 'f', and 'DC' mean the transmitter side, receiver side, LC filter, and DC filter, respectively. I_{rect} is the output current of the rectifier which is used in the current feedback control.

The circuit parameters of the double-sided LCC WPT part are decided so that the following equation is satisfied:

$$\omega = \frac{1}{\sqrt{L_1 C_1}} = \frac{1}{\sqrt{L_2 C_2}} = \frac{1}{\sqrt{L_{\mathrm{f1}} \frac{C_1 C_{\mathrm{f1}}}{C_1 + C_{\mathrm{f1}}}}} = \frac{1}{\sqrt{L_{\mathrm{f2}} \frac{C_2 C_2}{C_2 + C_{\mathrm{f2}}}}}, \tag{1}$$

where ω denotes the resonant angular frequency.

III. Pulse Density Modulation

This section explains the PDM for the receiver-side rectification. In the PDM operation, the active rectifier is switched between a diode mode and short mode which are shown in Fig. 2. The mode change is done when the filter current i_{f2} becomes zero (zero current switching); therefore, the switching loss does not occur. Fig. 3 shows the ideal I_{rect} waveforms of two types of the PDM: centralized PDM (CPDM) and distributed PDM (DPDM) when the duty ratio is 0.5. T and T' are the resonance period which is $2\pi/\omega$ and the control period which is defined as the product of integer N and T, respectively. The pulses of the CPDM are put on one side, therefore, the implementation is very easy. However, the ripple of the receiver current I_2 becomes large. In addition, the period of the short mode becomes long, hence the filter current i_{f2} becomes large. As a result, some problems occur such as the heat and noise due to the magnetostriction in the filter inductor L_{f2}, and the EMC noise. On the other hand, the pulses of the DPDM are equally

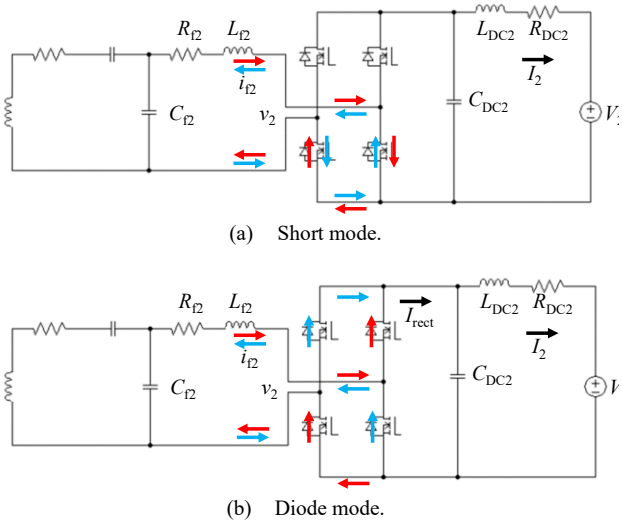

(a) Short mode.

(b) Diode mode.

Fig. 2. Two modes of the active rectifier in PDM.

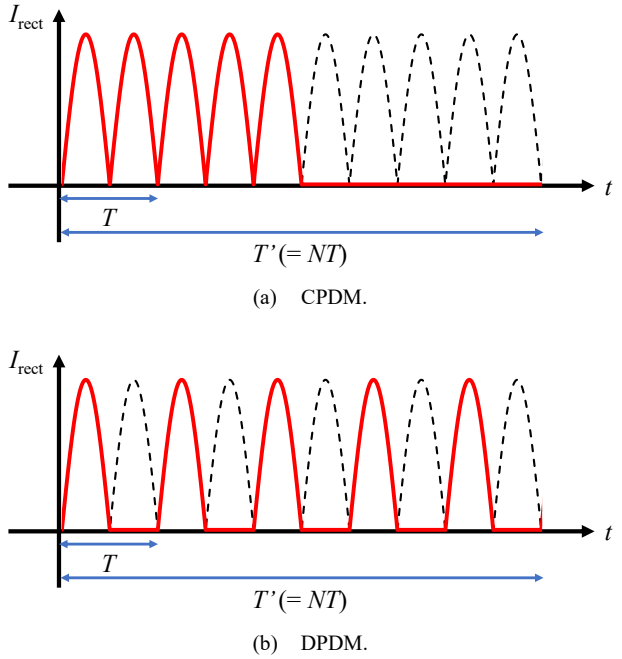

(a) CPDM.

(b) DPDM.

Fig. 3. Ideal I_{rect} waveforms. (Duty = 0.5)

put during the control period. The ripple of the receiver current and the amplitude of the filter current becomes smaller than ones of the CPDM because of the short period of the short mode. The energy efficiency evaluation of the CPDM and DPDM are experimentally conducted in this paper.

IV. Current Controller

This section describes the receiving current controller. Fig. 4 shows the block diagram of the current controller. It consists of two feedback loops to quickly control the receiver current I_2. The superscript 'ref' and 'res' denote the reference value and response value, respectively. The plant block means the DC filter plant model whose transfer function $P(s)$ is represented as

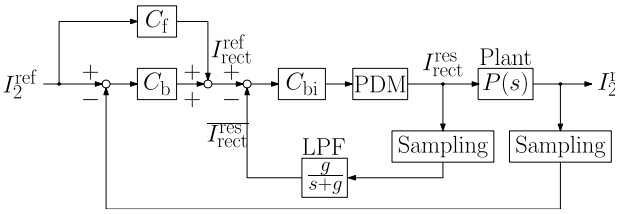

Fig. 4. Block diagram of the receiving current controller.

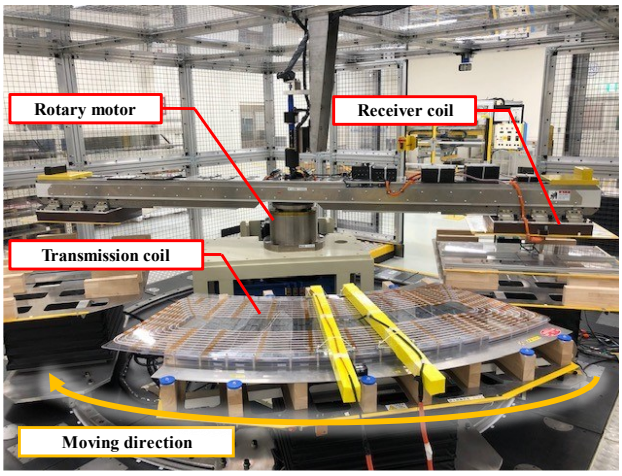

Fig. 5. High-speed rotational DWPT testbench (produced by TOYOTA MOTOR CORPORATION).

TABLE I. CIRCUIT PARAMETERS

Parameters	Symbols	Values
DC Voltage	V_1, V_2	220 V, 220 V
WPT inductance	L_1, L_2	194.8 μH, 279.4 μH
WPT resistance	R_1, R_2	385 mΩ, 1101 mΩ
WPT capacitance	C_1, C_2	18.0 nF, 12.6 nF
Filter inductance	L_{f1}, L_{f2}	25.5 μH, 51.0 μH
Filter resistance	R_{f1}, R_{f2}	68 mΩ, 50 mΩ
Filter capacitance	C_{f1}, C_{f2}	141 nF, 69.5 nF
DC filter inductance	L_{DC}	10 μH
DC filter inductance	R_{DC}	20 mΩ
DC filter inductance	C_{DC}	210 nF
Resonant frequency	$f(=\omega/2\pi)$	84.5 kHz
Number of pulses in T	N	10
Control frequency	$1/T$	8.45 kHz

$$P(s) = \frac{I_2}{I_{rect}} = \frac{1}{L_{DC2}C_{DC2}s^2 + R_{DC2}C_{DC2}s + 1}, \qquad (2)$$

where s denotes Laplace operator. In the inner loop, the rectified current I_{rect} is controlled using a PI feedback controller whose gains are $C_{bi}{}^p$ and $C_{bi}{}^i$. I_{rect} is a discontinuous waveform as shown in Fig. 3; therefore, a low pass filter whose cut-off frequency is g is utilized to smooth the waveform. In the outer loop, the receiver current is controlled using a feedforward controller whose gain is C_f and PI feedback controller whose gains are $C_b{}^p$ and $C_b{}^i$.

In the DWPT system, the receiver coil is not always on the transmitter coil. In the experiments, the current reference $I_2{}^{ref}$ is set at a constant. When the receiving current becomes zero, the integration term in the PI controllers gradually increases and the duty input saturates. In order to prevent the saturation, an anti-windup control is utilized in the integration part.

TABLE II. CONTROL PARAMETERS

Parameters	Symbols	Values
Feedforward controller gain	C_f	1
Inner feedback controller gains	$C_{bi}{}^p$	0.339
	$C_{bi}{}^i$	2025
Outer feedback controller gains	$C_{bi}{}^p$	1
	$C_{bi}{}^i$	10
Cut-off frequency	g	8500 rad/s

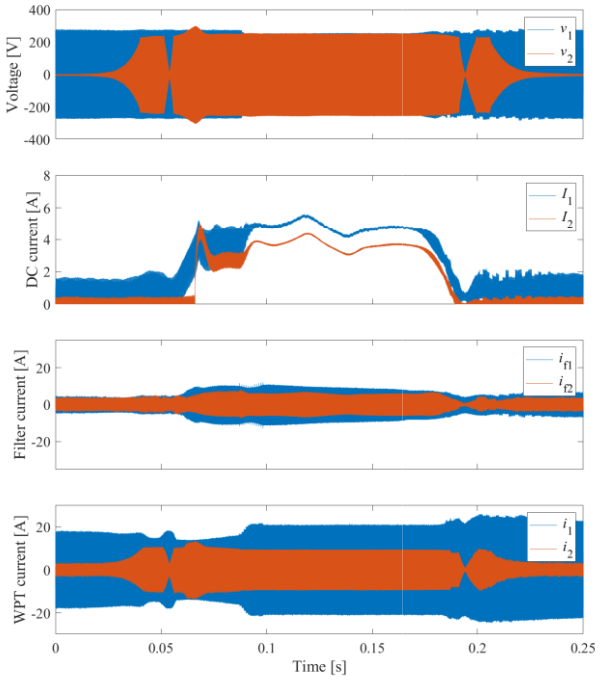

Fig. 6. Experimental results when the rectifier works as in the diode mode (40 km/h).

V. EXPERIMENTS

This section describes the experimental results of the receiving current control using two types of PDM and evaluates the efficiency. Fig. 5 shows the high-speed rotational DWPT testbench used in the experiments. At the tip of the top bar, the receiver coil is installed. The transmitter coil is fixed on the ground. The DWPT test situation can be reproduced by rotating the center motor at high speed. The circuit parameters and control parameters are listed in Tables I and II, respectively. The control parameters are experimentally decided. The pulse pattern of the DPDM is listed in a table in advance. In the experiments, the DWPT situation with 40 km/h vehicle speed is reproduced.

Firstly, the experimental results when the active rectifier always works as in the diode mode is described. Fig. 6 shows the experimental results. The blue and orange lines denote the measured values of the transmitter and receiver sides, respectively. From the top figure, the high-frequency voltage,

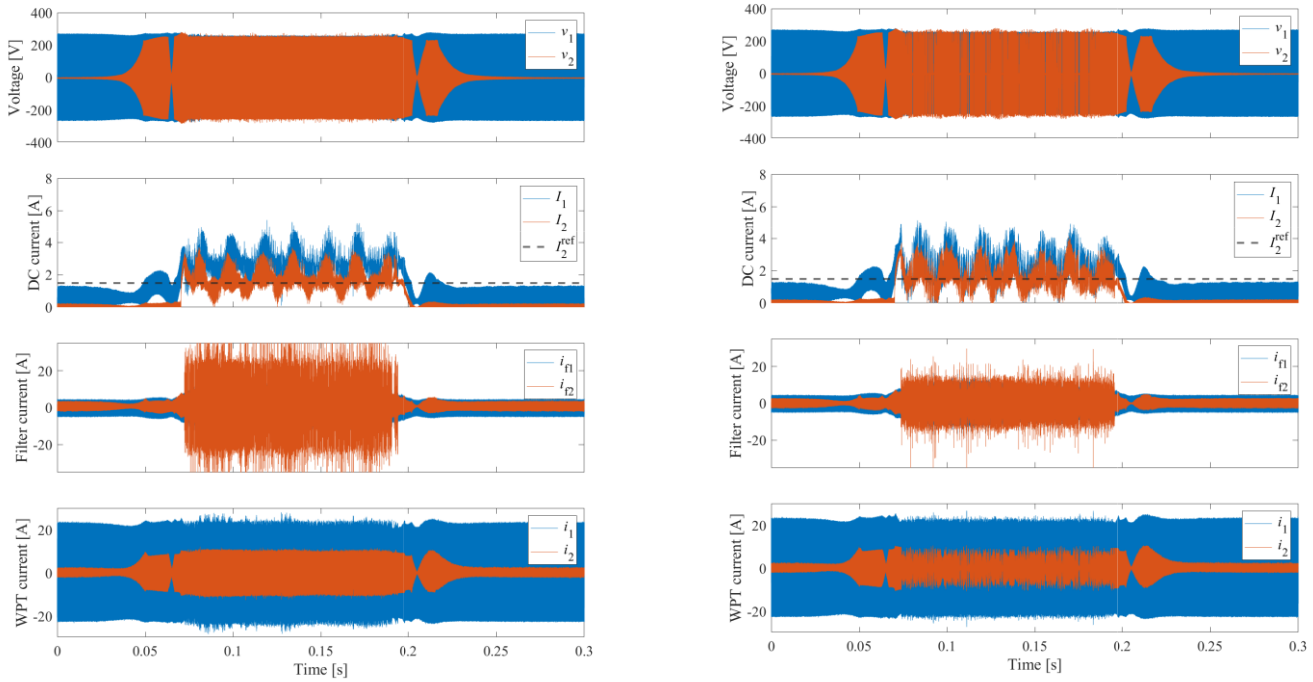

(a) CPDM. (b) DPDM.

Fig. 7. Experimental results of the receiving current control when I_2^{ref} = 1.5 A (40 km/h).

TABLE III. CALCULATED ENERGY AND ENERGY EFFICIENCY IN DWPT EXPERIMENTS

Diode mode			
I_2^{ref} [A]	E_1 [Ws]	E_2 [Ws]	η [%]
–	115.9	86.8	74.9
CPDM			
1.0	60.5	28.4	46.9
1.5	73.8	43.0	58.3
2.0	86.1	56.1	65.1
DPDM			
1.0	45.6	25.0	54.8
1.5	67.2	43.2	64.2
2.0	83.6	57.2	68.4

DC current, filter current, and WPT current are displayed. From the DC current waveform, it was confirmed that the receiving current I_2 is changed due to the mutual inductance dynamic change. The constant current characteristics by the double-sided LCC topology can be confirmed from the WPT current response i_2 [11].

Next, Fig. 7 shows the experimental results of the current control using the CPDM and DPDM when the receiving current reference I_2^{ref} is set at 1.5 A. The meanings of the lines and figures are the same in Fig. 6. From the response of the receiving current I_2, it is confirmed that the current is controlled at the reference value which is displayed as the black dot line. Both the calculated mean values of the receiving current using the CPDM and DPDM from 0.09 s to 0.19 s are 1.58 A which is 5.3% error of the reference. The periodic oscillation is observed in the DC current response. It may be a noise by the commercial power supply because the frequency is 50 Hz.

Finally, the transmission energy efficiency is evaluated. The transmission energy can be calculated by integrating the products of the DC voltage and current. The transmission energy efficiency η is derived as

$$\eta = \frac{E_2\ [\mathrm{Ws}]}{E_1\ [\mathrm{Ws}]} = \frac{\int_{t_s}^{t_f} V_2 I_2 dt}{\int_{t_s}^{t_f} V_1 I_1 dt}, \tag{3}$$

where t_s and t_f are the WPT start time and end time, respectively. The calculated energy and energy efficiency are listed in Table III when the current reference I_2^{ref} is set at 1.0 A, 1.5 A, and 2.0 A. As a result, the energy efficiency of the DPDM is 3.3–7.9% higher than one of the CPDM, especially in the case when the current reference is small. The reason is that the loss in the receiver-side filter is large because i_{f2} is large when the CPDM is used as shown in Fig. 7(a).

VI. CONCLUSIONS

This paper evaluated the receiving current control using the CPDM and DPDM from the viewpoint of the transmission energy efficiency. The control performances were compared by the experiments using the high-speed rotational DWPT testbench. It was confirmed that the receiving current followed to the reference value with 5.3% error using both the CPDM and DPDM in spite of the mutual inductance dynamic change at 40 km/h speed. On the other hand, the energy efficiency of the DPDM was 3.3–7.9% higher than one of the CPDM because the DPDM could suppress the increase of the filter current in the short mode. Therefore, the DPDM is effective for the receiving current control of the DWPT system.

REFERENCES

[1] O. Shimizu, S. Nagai, T. Fujita, and H. Fujimoto, "Potential for CO2 reduction by dynamic wireless power transfer for passenger vehicles in Japan", *Energies*, vol. 13. no. 3342, pp. 1–15, 2020.

[2] S. Laporte, G. Coquery, V. Deniau, A. D. Bernardinis, and N. Hautiere, "Dynamic wireless power transfer charging infrastructure for future EVs: from experimental track to real circulated roads demonstrations", *World Electric Vehicle Journal*, vol. 10, no. 84, pp. 1–22, 2019.

[3] D. Gunji, Y. Mukai, T. Imura, and H. Fujimoto, "Basic study on arrangement design of in-motion charging facility on urban roads", in *Proc. 44th Annual Conference of the IEEE Ind. Electron. Society*, pp. 5153–5158, 2018.

[4] H. Zhu, B. Zhang, and L. Wu, "Output power stabilization for wireless power transfer system employing primary-side-only control", *IEEE Access*, vol. 8, pp. 63735–63747, 2020.

[5] Z. Zhou, L. Zhang, Z. Liu, Q. Chen, R. Long, and H. Su, "Model predictive control for the receiving-side DC-DC converter of dynamic wireless power transfer", *IEEE Trans. Power Electron.*, vol. 35, no. 9, pp. 8985–8997, 2020.

[6] G. Lovison, T. Imura, H. Fujimoto, and Y. Hori, "Secondary-side-only phase-shifting voltage stabilization control with a single converter for WPT systems with constant power load", *IEEJ Journal of Industry Applications*, vol. 8, no. 1, pp. 66–74, 2019.

[7] H. Matsumoto, T. Zaitsu, R. Noborikawa, Y. Shibako, and Y. Neba, "Control for maximizing efficiency of three-phase wireless power transfer systems at misalignments", *IEEJ Journal of Industry Applications*, vol. 9, no. 4, pp. 401–407, 2020.

[8] *Wire-less power transfer for light-duty plug-in/electric vehicles and alignment methodology*, Society of Automotive Engineers International recommended practice J2954, 2020.

[9] S. Chen, H. Li, and Y. Tang, "Extending the operating region of inductive power transfer systems through dual-side cooperative control", *IEEE Trans. Ind. Electron.*, vol. 67, no. 11, pp. 9302–9312, 2020.

[10] M. Khalilian and P. Guglielmi, "Primary-side control of a wireless power transfer system with double-sided LCC compensation topology for electric vehicle battery charging", in *Proc. IEEE International Telecommunications Energy Conference*, 2018.

[11] P. S. R. Nayak and D. Kishan, "Performance analysis of series/parallel and dual side LCC compensation topologies of inductive power transfer for EV battery charging system", *Frontiers in Energy*, no. 14, pp. 166–179, 2018.